

Theoretical study of the insulating oxides and nitrides: SiO₂, GeO₂, Al₂O₃, Si₃N₄, and Ge₃N₄

C. Sevik* and C. Bulutay†

Department of Physics and Institute of Materials Science and Nanotechnology
Bilkent University, Ankara, 06800, Turkey

(Dated: March 23, 2022)

An extensive theoretical study is performed for wide bandgap crystalline oxides and nitrides, namely, SiO₂, GeO₂, Al₂O₃, Si₃N₄, and Ge₃N₄. Their important polymorphs are considered which are for SiO₂: α -quartz, α - and β -cristobalite and stishovite, for GeO₂: α -quartz, and rutile, for Al₂O₃: α -phase, for Si₃N₄ and Ge₃N₄: α - and β -phases. This work constitutes a comprehensive account of both electronic structure and the elastic properties of these important insulating oxides and nitrides obtained with high accuracy based on density functional theory within the local density approximation. Two different norm-conserving *ab initio* pseudopotentials have been tested which agree in all respects with the only exception arising for the elastic properties of rutile GeO₂. The agreement with experimental values, when available, are seen to be highly satisfactory. The uniformity and the well convergence of this approach enables an unbiased assessment of important physical parameters within each material and among different insulating oxide and nitrides. The computed static electric susceptibilities are observed to display a strong correlation with their mass densities. There is a marked discrepancy between the considered oxides and nitrides with the latter having sudden increase of density of states away from the respective band edges. This is expected to give rise to excessive carrier scattering which can practically preclude bulk impact ionization process in Si₃N₄ and Ge₃N₄.

PACS numbers: 61.50.Ah, 62.20.Dc, 71.20.-b, 71.20.Ps, 77.22.Ch

I. INTRODUCTION

Insulating oxides and nitrides are indispensable materials for diverse applications due to their superior mechanical, thermal, chemical and other outstanding high temperature properties. Furthermore, in the electronic industry these wide band gap materials are being considered for alternative gate oxides¹ and in the field of integrated optics they provide low-loss dielectric waveguides². Recently the subject of wide bandgap oxides and nitrides have gained interest within the context of nanocrystals which offer silicon-based technology for light emitting devices and semiconductor memories³. These nanocrystals are embedded in an insulating matrix which is usually chosen to be silica^{4,5,6,7}. However, other wide bandgap materials are also employed such as germania^{8,9}, silicon nitride^{10,11,12}, and alumina^{13,14,15}. As a matter of fact, the effect of different host matrices is an active research topic in this field.

Among these insulating oxides and nitrides technologically most important ones are SiO₂, Al₂O₃, Si₃N₄. The activity around GeO₂ is steadily increasing. Another closely-related material, Ge₃N₄ has attracted far less attention up to now even though it has certain interesting properties¹⁶. The major obstacle has been the sample growth. However, a very recent study reported an *in situ* Ge₃N₄ growth on Ge, demonstrating high thermal stability and large band offsets with respect to the Ge system¹⁷. In this comprehensive work, we present the *ab initio* structural and electronic properties of all these materials considering their common polymorphs; these are for SiO₂: α -quartz, α - and β -cristobalite and stishovite

phases, for GeO₂: α -quartz, and rutile phases, for Si₃N₄ and Ge₃N₄: α - and β -phases and for Al₂O₃: α -phase. For amorphous and inherently imperfect matrices, these perfect crystalline phases serve as important reference systems. Moreover, due to their distinct advantages, *epitaxial* host lattices are preferred over the amorphous ones for specific applications.

With an eye on these technological applications, we focus on several physical properties of these lattices. The elastic constants play an important role on the strain profile of the embedded core semiconductor. Using Eshelby's continuum elastic consideration¹⁸ the radial and tangential stress fields of the nanocrystal can be determined¹⁹; these in turn, affect the optical properties⁶. The static and optical dielectric constants of these lattices introduce nontrivial local field effects that modify the absorption spectra of an isolated nanocrystal when embedded inside one of these matrices²⁰. Based on the simple effective medium theory which has been tested by *ab initio* calculations²¹, one can assess which host lattice and nanocrystal combination would possess the desired optical properties. Because of the dielectric mismatch between the nanocrystal core and the surrounding lattice, image charges will be produced²². These image charges should be taken into account in characterizing nanocrystal excitons²³. Another promising application is the visible and near infrared electroluminescence from Si and Ge nanocrystals³. The electroluminescence is believed to be achieved by the recombination of the electron hole pairs injected to nanocrystals under high bias³. In this context the bulk state impact ionization process which can also give rise to electroluminescence is considered to be

detrimental leading to dielectric breakdown. For high-field carrier transport, the crucial physical quantity was identified to be the valence and conduction band density of states (DOS) for each of the crystalline polymorph²⁴. Based on these technology-driven requirements we compute the elastic constants, band structures, dielectric permittivities and electronic DOS of these aforementioned crystal polymorphs. Our *ab initio* framework is based on the density functional theory^{25,26}, using pseudopotentials and a plane wave basis²⁷. With the exception of Ge_3N_4 which was far less studied, vast amount of theoretical work is already available spread throughout the literature based on a variety of techniques^{28,29,30,31,32,33,34,35,36,37}. Our first-principles study here enables a uniform comparison of important physical parameters within each material and among different insulating oxides and nitrides.

The plan of the paper is as follows: in Sec. II we provide details of our *ab initio* computations, Sec. III contains our first-principles results for the structural, electronic properties of the materials considered followed by our conclusions in Sec. IV.

II. DETAILS OF AB INITIO COMPUTATIONS

Structural and electronic properties of the polymorphs under consideration have been calculated within the density functional theory^{25,26}, using the plane wave basis pseudopotential method as implemented in the ABINIT code²⁷. The results are obtained under the local density approximation (LDA) where for the exchange-correlation interactions we use the Teter Pade parameterization³⁸, which reproduces Perdew-Zunger³⁹ (which reproduces the quantum Monte Carlo electron gas data of Ceperley and Alder⁴⁰). We tested the results under two different norm-conserving Troullier and Martins⁴¹ type pseudopotentials, which were generated by A. Khein and D.C. Allan (KA) and Fritz Haber Institute (FHI). For both pseudopotentials, the valence configurations of the constituent atoms were chosen as $\text{N}(2s^2p^3)$, $\text{O}(2s^2p^4)$, $\text{Al}(3s^23p^1)$, $\text{Si}(3s^23p^2)$, and $\text{Ge}(4s^24p^2)$. The number of angular momenta of the KA (FHI) pseudopotentials and the chosen local channel were respectively, for N: 1, p (3, d), for O: 1, p (3, d), for Al: 2, d (3, d), for Si: 2, d (3, d), and for Ge: 1, p (3, s). Our calculated values for these two types of pseudopotentials were very similar, the only exceptional case being the elastic constants for rutile GeO_2 . Dielectric permittivity and the fourth-order tensor of elastic constants of each crystal are determined by starting from relaxed unit cell under the application of finite deformations within density functional perturbation theory⁴² as implemented in ABINIT and ANADD8 extension of it. Another technical detail is related with the element and angular momentum-resolved partial density of states (PDOS). To get a representative PDOS behavior we need to specify the spherical regions situated around each relevant atomic site. The radii of these spheres are chosen to partition the

bond length in proportion to the covalent radii of the constituent atoms. This resulted in the following radii: for the α -quartz SiO_2 , $r_{\text{Si}} = 0.97 \text{ \AA}$, $r_{\text{O}} = 0.65 \text{ \AA}$, for the rutile GeO_2 , $r_{\text{Ge}} = 1.16 \text{ \AA}$, $r_{\text{O}} = 0.69 \text{ \AA}$, for the α - Al_2O_3 , $r_{\text{Al}} = 1.32 \text{ \AA}$, $r_{\text{O}} = 0.56 \text{ \AA}$, and for the β - Si_3N_4 , $r_{\text{Si}} = 1.03 \text{ \AA}$, $r_{\text{N}} = 0.70 \text{ \AA}$. It should be pointed that even though such an approach presents a good relative weight of the elements and angular momentum channels, it inevitably underestimates the total DOS, especially for the conduction bands. Other details of the computations are deferred to the discussion of each crystal polymorph.

III. FIRST-PRINCIPLES RESULTS

First, we address the general organization and the underlying trends of our results. The lattice constants and other structural informations of all crystals are listed in Table I. Table II contains the bond lengths and bond angles of the optimized oxide polymorphs. These results can be used to identify the representation of each polymorph within the amorphous oxides⁵². The elastic constants and dielectric permittivity tensor of each crystal are tabulated in Table III and Table IV, respectively. Very close agreement with the existing experimental data and previous calculations can be observed which gives us confidence about the accuracy and convergence of our work. Employing KA pseudopotentials, the band structure for the crystals are displayed along the high-symmetry lines in Figs. 1,3,5,6 together with their corresponding total DOS. Such an information is particularly useful in the context of high-field carrier transport. These results are in good agreement with the previous computations^{29,32,35,36}. For all of the considered polymorphs the conduction band minima occur at the Γ point whereas the valence band maxima shift away from this point for some of the phases making them indirect band gap matrices (see Table V). However, the direct band gap values are only marginally above the indirect band gap values. These LDA band gaps are underestimated which is a renown artifact of LDA for semiconductors and insulators⁵⁹. In this work we do not attempt any correction procedure to adjust the LDA band gap values.

We present in Figs. 2,4,7 the element- and angular momentum-resolved PDOS. A common trend that can be observed in these various lattices is that their valence band maxima are dominated by the p states belonging to O atoms; in the case of Si_3N_4 and Ge_3N_4 they are the N atoms. For the conduction band edges, both constituent elements have comparable contribution. This parallels the observation in amorphous SiO_2 where due to large electronegativity difference between Si and O, the bonding orbitals have a large weight on O atoms whereas the lowest conduction band states with antibonding character have a significant contribution from the Si atoms⁶⁰.

From another perspective, the band structures and the associated DOS reveal that there is a marked discrepancy between the valence and conduction band edges where for

TABLE I: Structural information on crystals.

| Crystal | Crystal Structure | Lattice Constants (Å) | Space Group | Molecules Per Prim. Cell | Density (gr/cm ³) |
|--|--------------------------|--|-------------|--------------------------|-------------------------------|
| α -quartz SiO ₂ | Hexagonal | $a = 4.883^a$ 4.854 ^b 4.913 ^c $c = 5.371^a$ 5.341 ^b 5.405 ^c | $P3_221$ | 3 | 2.698 |
| α -cris. SiO ₂ | Tetragonal | $a = 4.950^a$ 4.939 ^b 4.973 ^c $c = 6.909^a$ 6.894 ^b 6.926 ^c | $P4_12_12$ | 4 | 2.372 |
| β -cris. SiO ₂ | Cubic | $a = 7.403^a$ 7.330 ^b 7.160 ^c | $Fd3m$ | 2 | 1.966 |
| Stishovite SiO ₂ | Tetragonal | $a = 4.175^a$ 4.145 ^b 4.179 ^d $c = 2.662^a$ 2.643 ^b 2.665 ^d | $P4_2/mnm$ | 2 | 4.298 |
| α -quartz GeO ₂ | Hexagonal | $a = 4.870^a$ 4.861 ^b 4.984 ^f $c = 5.534^a$ 5.520 ^b 5.660 ^f | $P3_221$ | 3 | 4.612 |
| Rutile GeO ₂ | Tetragonal Tetragonal | $a = 4.283^a$ 4.314 ^b 4.4066 ^g $c = 2.782^a$ 2.804 ^b 2.8619 ^g | $P4_2/mnm$ | 2 | 6.655 |
| α -Al ₂ O ₃ | Rhombohedral | $a = 4.758^a$ 4.762 ^e $c = 12.98^a$ 12.896 ^e | $R\bar{3}c$ | 2 | 3.992 |
| α -Si ₃ N ₄ | Hexagonal | $a = 7.732^a$ 7.766 ⁱ $c = 5.603^a$ 5.615 ⁱ | C_{3v}^4 | 4 | 3.211 |
| β -Si ₃ N ₄ | Hexagonal | $a = 7.580^a$ 7.585 ^j $c = 2.899^a$ 2.895 ^j | C_{6h}^2 | 2 | 3.229 |
| α -Ge ₃ N ₄ | Hexagonal | $a = 7.985^a$ $c = 5.786^a$ | C_{3v}^4 | 4 | 5.691 |
| β -Ge ₃ N ₄ | Hexagonal | $a = 7.826^a$ $c = 2.993^a$ | C_{6h}^2 | 2 | 5.727 |

^aThis Work KA^bThis Work FHI^cRef. 43^dRef. 44^fRef. 45^gRef. 46,47^eRef. 31ⁱRef. 32^jRef. 37TABLE II: Bond lengths and bond angles (in degrees) of SiO₂ and GeO₂ polymorphs where x represents a Si or a Ge atom.

| Crystal | | x-O (Å) | x-O (Å) | O-x-O | O-x-O | O-x-O | O-x-O | x-O-x | x-O-x |
|-----------------------------------|-------------------|---------|---------|--------|--------|--------|--------|--------|--------|
| α -quartz SiO ₂ | This Work | 1.613 | 1.618 | 110.75 | 109.32 | 109.07 | 108.47 | 140.55 | |
| | Exp. ^a | 1.605 | 1.614 | 110.50 | 109.20 | 109.00 | 108.80 | 143.7 | |
| α -quartz GeO ₂ | This Work | 1.693 | 1.699 | 113.03 | 110.62 | 107.94 | 106.16 | 130.56 | |
| α -cris. SiO ₂ | This Work | 1.597 | 1.596 | 111.59 | 110.08 | 109.03 | 108.02 | 146.02 | |
| | Exp. ^b | 1.603 | 1.603 | 111.40 | 110.00 | 109.00 | 108.20 | 146.5 | |
| β -cris. SiO ₂ | This Work | 1.603 | | 109.47 | | | | 180 | |
| | Exp. ^c | 1.611 | | 107.80 | | | | 180.00 | |
| Stishovite SiO ₂ | This Work | 1.804 | 1.758 | 98.47 | 81.53 | | | 130.76 | 98.47 |
| | Exp. ^d | 1.760 | 1.810 | | | | | 130.60 | |
| Rutile GeO ₂ | This Work | 1.848 | 1.824 | 99.34 | 80.66 | | | 99.34 | 130.33 |

^aRef. 48^bRef. 49^cRef. 50^dRef. 51

the former there occurs a sharp increase of DOS just below the band edge. As the probabilities of most scattering processes are directly proportional to DOS⁶¹, in the case of high-field carrier transport the electrons should encounter far less scatterings and hence gain much higher energy from the field compared to holes. In this respect

Si₃N₄ and Ge₃N₄ are further different from the others where for both conduction and valence bands the DOS dramatically increases (cf. Fig. 6) so that the carriers should suffer from excessive scatterings which practically precludes the bulk impact ionization for this material.

Another common trend can be investigated between

TABLE III: Elastic constants and bulk modulus for each crystal.

| Crystal | (GPa) | C_{11} | C_{12} | C_{13} | C_{14} | C_{33} | C_{44} | C_{66} | B |
|--|-------------------|----------|----------|----------|----------|----------|----------|----------|-----|
| α -quartz SiO ₂ | KA | 76.2 | 11.9 | 11.2 | -17.0 | 101.7 | 54.0 | 32.1 | 35 |
| | FHI | 79.5 | 9.73 | 9.54 | -18.9 | 101.7 | 55.5 | 34.9 | 35 |
| | Exp. ^a | 87.0 | 7.00 | 13.0 | -18.0 | 107.0 | 57.0 | 40.0 | 38 |
| | Exp. ^b | 87.0 | 7.00 | 19.0 | -18.0 | 106.0 | 58.0 | | 40 |
| α -Cris. SiO ₂ | KA | 49.30 | 5.26 | -11.41 | | 44.78 | 74.15 | 26.85 | 12 |
| β -Cris. SiO ₂ | KA | 194.0 | 135.0 | | | | 82.67 | | 155 |
| | FHI | 196.1 | 134.2 | | | | 85.40 | | 155 |
| Stishovite SiO ₂ | KA | 447.7 | 211.0 | 203.0 | | 776.0 | 252.0 | 302.0 | 306 |
| | FHI | 448.8 | 211.1 | 191.0 | | 752.0 | 256.5 | 323.0 | 302 |
| | Exp. ^c | 453.0 | 211.0 | 203.0 | | 776.0 | 252.0 | 302.0 | 308 |
| α -quartz GeO ₂ | KA | 66.7 | 24.3 | 23.1 | -3.00 | 118.7 | 41.3 | 21.2 | 41 |
| | FHI | 63.8 | 25.7 | 26.2 | -0.81 | 120.2 | 35.3 | 19.1 | 42 |
| | Exp. ^d | 66.4 | 21.3 | 32.0 | -2.20 | 118.0 | 36.8 | 22.5 | 42 |
| | Exp. ^b | 64.0 | 22.0 | 32.0 | -2.00 | 118.0 | 37.0 | 21.0 | 42 |
| Rutile GeO ₂ | KA | 405.9 | 235.3 | 189.2 | | 672.4 | 206.0 | 314.4 | 292 |
| | FHI | 349.2 | 197.2 | 185.1 | | 617.5 | 171.8 | 274.8 | 258 |
| | Exp. ^e | 337.2 | 188.2 | 187.4 | | 599.4 | 161.5 | 258.4 | 251 |
| α -Al ₂ O ₃ | KA | 493.0 | 164.1 | 130.1 | | 485.8 | 155.5 | 164.4 | 258 |
| | Exp. ^f | 497.0 | 164.0 | 111.0 | | 498.0 | 147.0 | | 251 |
| β -Si ₃ N ₄ | KA | 421.8 | 197.8 | 116.6 | | 550.7 | 100.2 | 112.0 | 250 |
| | Exp. ^g | 433.0 | 195.0 | 127.0 | | 574.0 | 108.0 | 119.0 | 259 |
| | Exp. ^h | 439.2 | 181.8 | 149.9 | | 557.0 | 114.4 | 135.9 | 265 |
| β -Ge ₃ N ₄ | KA | 364.3 | 184.9 | 111.7 | | 486.3 | 80.4 | 89.7 | 225 |

^aRef. 53^bRef. 54^cRef. 55^dRef. 45^eRef. 47^fRef. 56^gRef. 57^hRef. 58

TABLE IV: Dielectric permittivity tensor.

| Crystal | $\epsilon_{xx}^0 = \epsilon_{yy}^0$ | ϵ_{zz}^0 | $\epsilon_{xx}^\infty = \epsilon_{yy}^\infty$ | ϵ_{zz}^∞ |
|--|-------------------------------------|-------------------|---|------------------------|
| α -quartz SiO ₂ | 4.643 | 4.847 | 2.514 | 2.545 |
| α -cris. SiO ₂ | 4.140 | 3.938 | 2.274 | 2.264 |
| β -cris. SiO ₂ | 3.770 | 3.770 | 2.078 | 2.078 |
| Stishovite SiO ₂ | 10.877 | 8.645 | 3.341 | 3.510 |
| α -quartz GeO ₂ | 5.424 | 5.608 | 2.864 | 2.947 |
| Rutile GeO ₂ | 10.876 | 8.747 | 3.679 | 3.945 |
| α -Al ₂ O ₃ | 10.372 | 10.372 | 3.188 | 3.188 |
| β -Si ₃ N ₄ | 8.053 | 8.053 | 4.211 | 4.294 |
| β -Ge ₃ N ₄ | 8.702 | 8.643 | 4.558 | 4.667 |

the density of each polymorph and the corresponding static permittivity, ϵ_s . Such a correlation was put forward by Xu and Ching among the SiO₂ polymorphs²⁹. We extend this comparison to all structures considered in this work and rather use $\chi_e = \epsilon_s - 1$ which corresponds to electric susceptibility. It can be observed from Fig. 8 that the trend established by SiO₂ polymorphs is also followed by β -Si₃N₄ and α -Al₂O₃. On the other hand, Ge-containing structures while possessing a similar trend among themselves, display a significant shift due to much higher mass of the this atom. This dependence on the

TABLE V: Indirect (E_g) and direct ($E_g(\Gamma)$) LDA Band Gaps for each crystal.

| Crystal | VB Max. | CB Min. | E_g (eV) | $E_g(\Gamma)$ (eV) |
|--|-------------|----------|------------|--------------------|
| α -quartz SiO ₂ | K | Γ | 5.785 | 6.073 |
| α -cris. SiO ₂ | Γ | Γ | 5.525 | 5.525 |
| β -cris. SiO ₂ | Γ | Γ | 5.317 | 5.317 |
| Stishovite SiO ₂ | Γ | Γ | 5.606 | 5.606 |
| α -quartz GeO ₂ | K | Γ | 4.335 | 4.434 |
| Rutile GeO ₂ | Γ | Γ | 3.126 | 3.126 |
| α -Al ₂ O ₃ | Γ | Γ | 6.242 | 6.242 |
| α -Si ₃ N ₄ | M | Γ | 4.559 | 4.621 |
| β -Si ₃ N ₄ | A- Γ | Γ | 4.146 | 4.365 |
| α -Ge ₃ N ₄ | M | Γ | 3.575 | 3.632 |
| β -Ge ₃ N ₄ | A- Γ | Γ | 3.447 | 3.530 |

atomic mass needs to be removed by finding a more suitable physical quantity. We should mention that such a correlation does not exist between the volume per primitive cell of each phase and the static permittivity. After these general comments, now we concentrate on the results of each lattice individually.

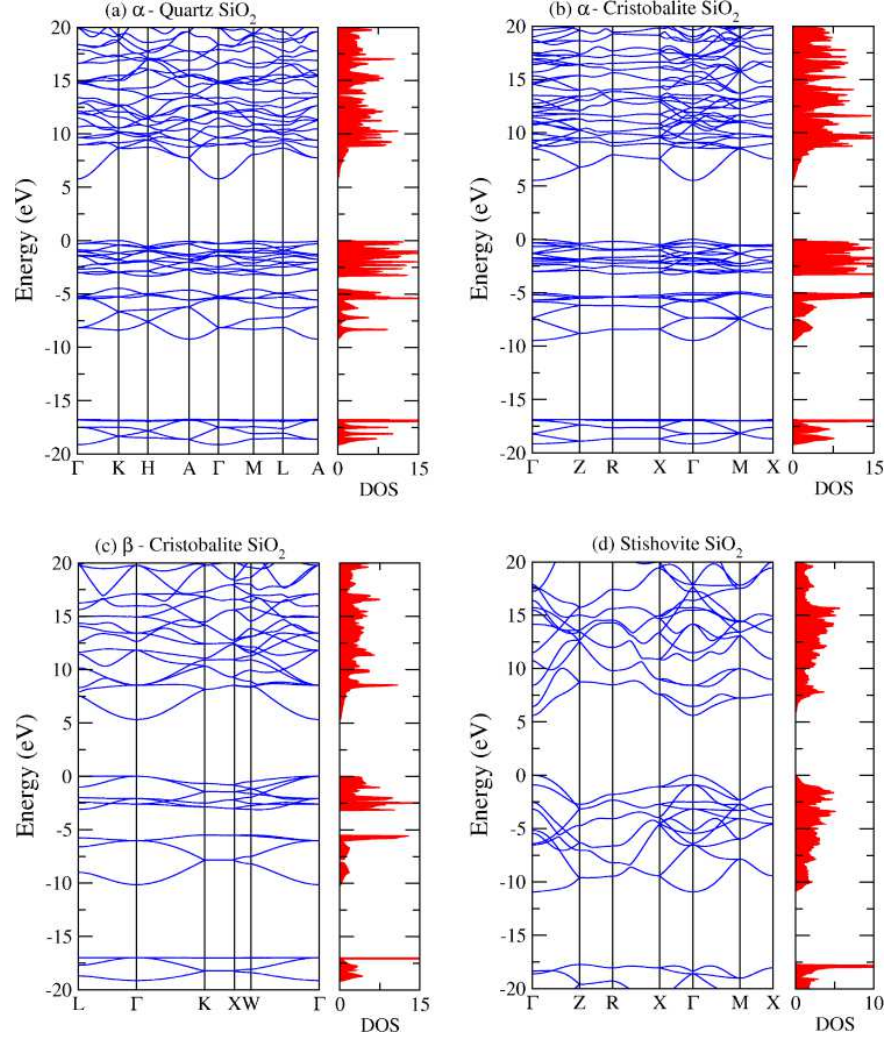


FIG. 1: LDA band structure and total DOS (electrons/eV cell) of (a) α -cristobalite SiO_2 , (b) α -quartz SiO_2 , (c) β -cristobalite SiO_2 , and (d) stishovite SiO_2 .

A. SiO_2

The α -quartz SiO_2 is one of the most studied polymorphs as it is the stable phase at the ambient pressure and temperature^{30,34}, furthermore its short-range order is essentially the same as the amorphous SiO_2 ⁶⁰. α -quartz SiO_2 has a hexagonal unit cell containing three SiO_2 molecules. A plane-wave basis set with an energy cutoff of 60 Ha was used to expand the electronic wave functions at the special k -point mesh generated by $10 \times 10 \times 8$ Monkhorst-Pack scheme⁶². The band structure of α -quartz SiO_2 has been calculated by many authors (see, for instance^{28,29}). Our calculated band structure and total DOS shown in Fig. 1(a) are in agreement with the published studies²⁹. The indirect LDA band gap for this crystal is 5.785 eV from the valence band maximum at K to the conduction band minimum at Γ . The direct LDA band gap at Γ is slightly larger than the indirect LDA band gap as seen in Table V. Calculated values of

the elastic constants and bulk modulus listed in Table III are in good agreement with the experiments. Apart from C_{12} , the elastic constants are within 10% of the experimental values. The discrepancy in C_{12} can be explained by the fact that C_{12} is very soft and this type of deviation also exists among experiments which is also the case for C_{14} .

α -cristobalite SiO_2 has a tetragonal unit cell containing four SiO_2 molecules. In the course of calculations an absolute energy convergence of 10^{-4} Ha was obtained by setting a high plane wave energy cutoff as 60 Ha and $10 \times 10 \times 8$ k -point sampling. Figure 1(b) shows the band structure of α -cristobalite SiO_2 with the 5.525 eV direct band gap at Γ . The bulk modulus of 12 GPa is the smallest among all the host lattice polymorphs considered in this work.

Regarding β -cristobalite, its actual structure is somewhat controversial, as a number of different symmetries have been proposed corresponding to space groups

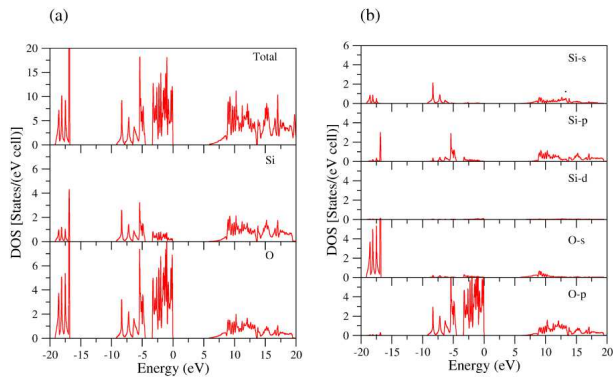


FIG. 2: DOS of α -quartz SiO_2 (a) Element-resolved; total, PDOS of Si, PDOS of O. (b) Angular momentum-resolved; Si s electrons, Si p electrons, Si d electrons (not visible at the same scale), O s electrons, O p electrons.

$Fd3m$, $I\bar{4}2d$, and $P2_13^{34}$. Recently, incorporating the quasiparticle corrections the tetragonal $I\bar{4}2d$ phase was identified to be energetically most stable⁶³. However, we work with the structure having the space group of $Fd3m$ that was originally proposed by Wyckoff⁶⁴ and which is widely studied primarily due to its simplicity^{28,30}. This phase has a cubic conventional cell with two molecules. We used 60 Ha plane wave energy cutoff and $10 \times 10 \times 10$ k -point sampling. Figure 1(c) shows the band structure of β -cristobalite SiO_2 with the 5.317 eV direct band gap at Γ . Unlike their band structures, total DOS of α - and β -cristobalite SiO_2 are very similar (cf. Fig. 1(c)). This similarity can be explained by the fact that their local structure are very close. On the other hand there is a considerable difference between the DOS spectra of the α -quartz SiO_2 and the β -cristobalite SiO_2 . In Table III, we present elastic constants of the β -cristobalite SiO_2 calculated by two types of pseudopotentials, FHI and KA. There is no considerable difference between them. Dielectric constants of β -cristobalite SiO_2 are the smallest among the five polymorphs of SiO_2 studied here (see Table IV).

Stishovite is a dense polymorph of SiO_2 with octahedrally coordinated silicon, unlike the previous phases³⁴. It has a tetragonal cell with two molecules. Calculations were done by using 60 Ha plane wave energy cutoff and $8 \times 8 \times 10$ k -point sampling. The band structure of stishovite with a wide single valence band is markedly different from that of the previous three crystalline phases of SiO_2 having two narrow upper valence bands. The cause of this increased valence bandwidth is the lack of separation between bonding and nonbonding states³⁶. Hence, the total DOS for stishovite shows no gap at the middle of the valence band (see Fig. 1(d)). Our calculations yield a direct LDA band gap of 5.606 eV at Γ . As seen in Table III, the differences between our computed elastic constants and the experimental values are less than 3%; this is an excellent agreement for LDA. Its bulk modu-

lus is the largest among all the host lattice polymorphs considered in this work. Moreover, dielectric constants of stishovite is the largest of the five polymorphs of SiO_2 considered in this work (see Table IV).

B. GeO_2

For α -quartz GeO_2 we used the same energy cutoff and k -point sampling as with α -quartz SiO_2 which yields excellent convergence. The band structure of the α -quartz GeO_2 is displayed in Fig. 3(a). The similarity of the band structures of the α -quartz GeO_2 and the α -quartz SiO_2 is not surprising as they are isostructural. Similarly their total DOS resemble each other (cf. Fig. 3(a)). The indirect LDA band gap for this phase is 4.335 eV from the valence band maximum at K to the conduction band minimum at Γ . The direct band gap at Γ is slightly different from indirect band gap as seen in Table V. This gap is smaller than that of the α -quartz SiO_2 . The perfect agreement between calculated elastic constants of the α -quartz GeO_2 and experimental values^{45,54} can be observed in Table III.

The rutile structure of GeO_2 , also known as argutite⁶⁵ is isostructural with the stishovite phase of SiO_2 . The same energy cutoff and k -point sampling values as for stishovite yield excellent convergence. The direct LDA band gap at Γ for rutile- GeO_2 is less than that of stishovite with a value of 3.126 eV. The two upper valence bands are merged in the total DOS (see Fig. 3(b)) as in the case of stishovite. The increased valence bandwidth in the band structure can be explained by the same reason as in the case of stishovite. The results of the elastic constants calculated with KA type pseudopotential shown in Table III deviate substantially from the experiment whereas the agreement with the FHI pseudopotentials is highly satisfactory. The similarity of the dielectric constants of rutile GeO_2 and stishovite can be observed in Table IV.

C. Al_2O_3

Al_2O_3 is regarded as a technologically important oxide due to its high dielectric constant and being reasonably a good glass former after SiO_2 ¹. The α - Al_2O_3 (sapphire) has the rhombohedral cell with two molecules. Computations about Al_2O_3 were done by using 60 Ha plane wave energy cutoff and a total of 60 k -points within the Brillouin zone. Fig. 5 shows the computed band structure and total DOS of the α - Al_2O_3 . These are in excellent agreement with the previous calculation^{31,33}. For Al_2O_3 , minimum of the conduction band is at Γ and maximum of the valence band is at a point along $\Gamma - X$ close to the Γ point. The corresponding LDA band gap is 6.242 eV. Because of the very small difference between the direct and indirect band gaps, Al_2O_3 is considered as a direct band gap insulator. Measured band gap of this crystal

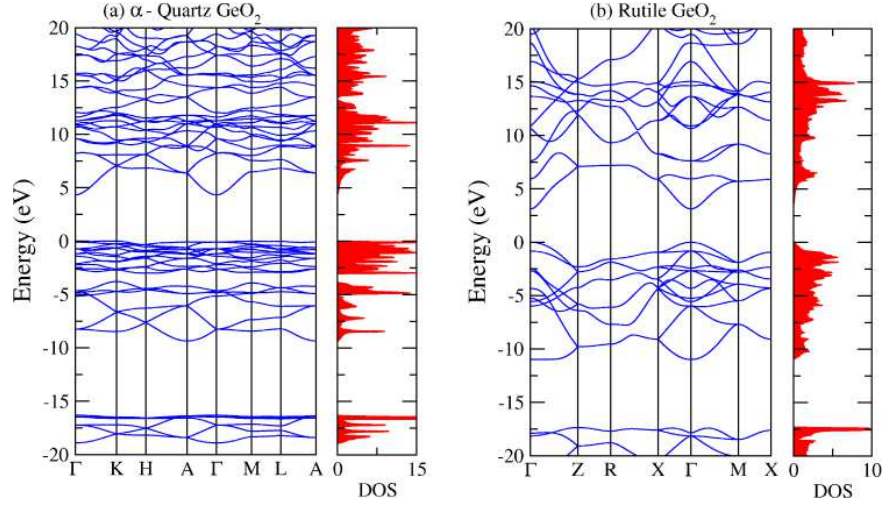


FIG. 3: LDA band structure and total DOS of (a) α -quartz GeO_2 , (c) rutile GeO_2 .

is 8.7 eV. However the precise value of the gap of Al_2O_3 is still elusive because of the existence of an excitonic peak near the absorbtions edge⁶⁶. As seen in Table III, computed values of the elastic constant and bulk modulus of Al_2O_3 are in excellent agreement with the experiments. As a further remark, the α - Al_2O_3 unit cell can be described as hexagonal or rhombohedral depending on the crystallographical definition of the space group $R\bar{3}C$. During our first-principles calculations it has been defined as rhombohedral in which case C_{14} vanishes. Although the sign of C_{14} is experimentally determined to be negative for the hexagonal- Al_2O_3 , previous calculations reported a positive value⁶⁷. To check this disagreement we have calculated the elastic constant of the hexagonal- Al_2O_3 and found it to be around -3.0.

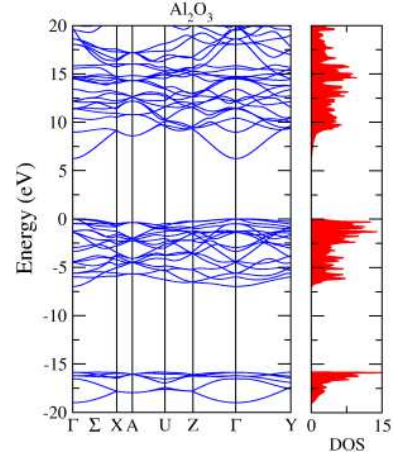


FIG. 5: LDA band structure and total DOS of α - Al_2O_3 .

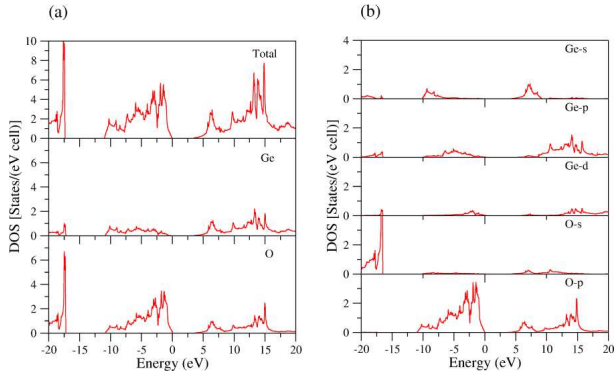


FIG. 4: DOS of rutile GeO_2 (a) Element-resolved; total PDOS of Ge, PDOS of O. (b) Angular momentum-resolved; Ge s electrons, Ge p electrons, Ge d electrons, O s electrons, O p electrons.

D. Si_3N_4 and Ge_3N_4

The research on silicon nitride has largely been driven by its use in microelectronics technology to utilize it as an effective insulating material and also as diffusion mask for impurities. Recently it started to attract attention both as a host embedding material for nanocrystals^{10,11,12} and also for optical waveguide applications². The α - and β - Si_3N_4 have hexagonal conventional cells with four and two molecules, respectively. We used 60 Ha plane wave energy cutoff and $6 \times 6 \times 8$ k -point sampling. The computed band structures of these two phases shown in Figs. 6 (a) and (b) are identical to those reported by Xu and Ching³². The top of the valence band for β - Si_3N_4 is along the Γ -A direction, and for α - Si_3N_4 it is at the M point. The bottom of the conduction band for two phases are at the Γ point. The direct and indi-

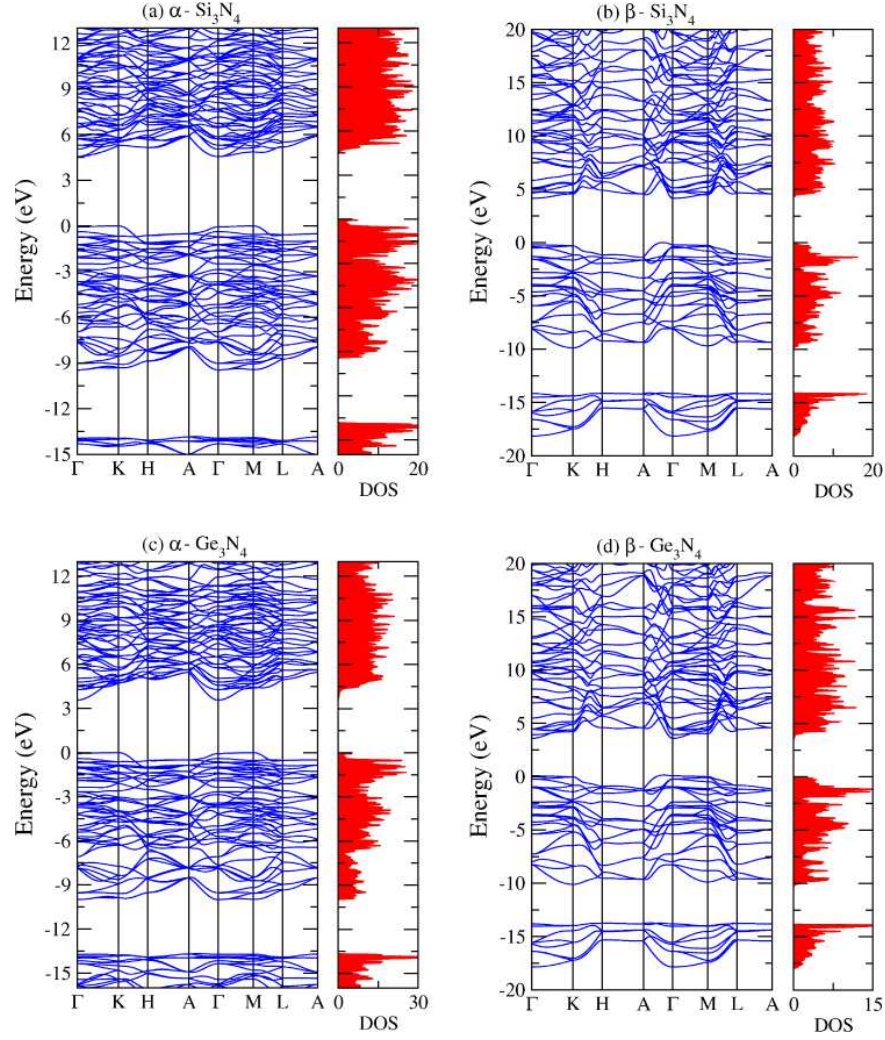


FIG. 6: LDA band structure and total DOS of (a) α - Si_3N_4 , (b) β - Si_3N_4 , (c) α - Ge_3N_4 and (d) β - Ge_3N_4 .

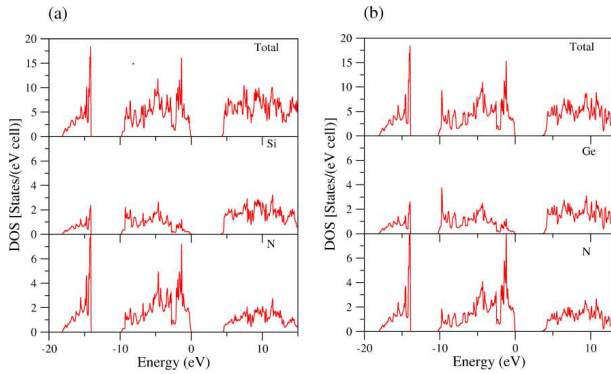


FIG. 7: Element-resolved DOS of (a) β - Si_3N_4 ; total, PDOS of Si, PDOS of N, (b) β - Ge_3N_4 ; total, PDOS of Ge, PDOS of N.

rect LDA band gaps of these two phases are respectively,

4.559 eV, 4.621 eV for α - Si_3N_4 and 4.146 eV, 4.365 eV for the β - Si_3N_4 . The general band structure of two phases are very similar, except that the α - Si_3N_4 has twice as many bands because the unit cell is twice as large. The total DOS of these two phases shown in Figs. 6(a) and (b) are only marginally different. Calculated values of the elastic constants and bulk modulus of β - Si_3N_4 listed in Table III are in excellent agreement with the quoted experiments. Those for the α - Si_3N_4 which is thermodynamically less stable with respect to β -phase⁶⁸ were left out due to excessive memory requirements for the desired accuracy.

Ge_3N_4 is the least studied material among the oxides and nitrides considered in this work. Recently its high-pressure γ -phase has attracted some theoretical interest⁶⁹. However, the available Ge_3N_4 samples contain a mixture of α and β -phases as in the case of Si_3N_4 and these are the polymorphs that we discuss in this work. The band structures of both of these phases of Ge_3N_4 (cf. Fig. 6) are very similar to those of Si_3N_4 . Regarding the

elastic constants of β - Ge_3N_4 , our theoretical results listed in Table III await experimental verification. In terms of density, the β phases of Si_3N_4 and Ge_3N_4 fill the gap between the α -quartz and stishovite/rutile phases of their oxides. As can be observed from Fig. 8 their electric susceptibility versus density behavior strengthens the correlation established by the remaining polymorphs. Finally it should be pointed that β - Ge_3N_4 has the largest high-frequency dielectric constant (ϵ_∞) among all the materials considered in this work.

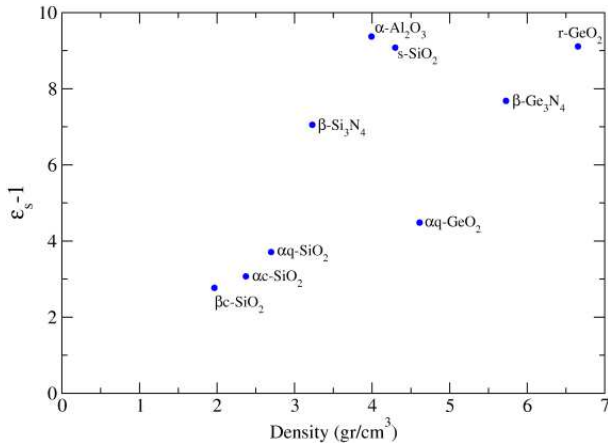


FIG. 8: Density versus direction-averaged static electric susceptibility.

IV. CONCLUSIONS

A comprehensive first-principles study is presented which is unique in analyzing common polymorphs of the

technologically-important insulating oxides and nitrides: SiO_2 , GeO_2 , Al_2O_3 , Si_3N_4 , and Ge_3N_4 . The structural parameters, elastic constants, static and optical dielectric constants are obtained in close agreement with the available results. The computed dielectric constants are observed to display a strong correlation with their mass densities. For all of the considered polymorphs the conduction band minima occur at the Γ point whereas the valence band maxima shift away from this point for some of the phases making them indirect band gap matrices. However, the direct band gap values are only marginally above the indirect band gap values. The investigation of band structure and DOS data reveal that the holes in all polymorphs considered and the electrons for the case of Si_3N_4 and Ge_3N_4 should suffer excessive scatterings under high applied field which will preclude bulk impact ionization for these carrier types and polymorphs. This can be especially important for applications vulnerable to dielectric breakdown.

A. Acknowledgments

This work has been supported by the European FP6 Project SEMINANO with the contract number NMP4 CT2004 505285. We would like to thank R. Eryiğit, T. Gürel, O. Gülseren, D. Çakır and T. Yıldırım for their useful advices and to Dr. Can Uğur Ayfer for the access to Bilkent University Computer Center facilities.

-
- * Electronic address: sevik@fen.bilkent.edu.tr
[†] Electronic address: bulutay@fen.bilkent.edu.tr
¹ J. Robertson, Rep. Prog. Phys. 69, (2006) 327.
² F. Ay and A. Aydinli, Opt. Matl. 26, (2004) 33.
³ S. Ossicini, L. Pavesi, and F. Priolo, *Light Emitting Silicon for Microphotonics*, (Springer, Berlin, 2003).
⁴ S. Hayashi, T. Nagareda, Y. Kanzawa, and K. Yamamoto, Jpn. J. Appl. Phys. 32, (1993) 3840.
⁵ F. Iacona, G. Franzó, C. Spinella, J. Appl. Phys. 87, (2000) 1295.
⁶ Y. Q. Wang, G. L. Kong, W. D. Chen, H. W. Diao, C. Y. Chen, S. B. Zhang, and X. B. Liao, Appl. Phys. Lett. 81, (2002) 4174.
⁷ U. Serincan, G. Aygun, and R. Turan, J. Lumin. 113, (2005) 229.
⁸ V. A. Volodin, E. B. Gorokhov, M. D. Efremov, D. V. Marin, and D. A. Orekhov, JETP Lett. 77, (2003) 411.
⁹ E. B. Gorokhov, V. A. Volodin, D. V. Marin, D. A. Orekhov, A. G. Cherkov, A. K. Gutakovskii, V. A. Shvets, A. G. Borisov, and M. D. Efremov, Semiconductors, 39,

- (2005) 1168.
¹⁰ V. A. Volodin, M. D. Efremov, and V. A. Gritsenko, Solid State Phenom. 57-58, (1997) 501.
¹¹ R. F. Steimle, M. Sadd, R. Muralidhar, R. Rao, B. Hradsky, S. Straub, and B. E. White, IEEE Trans. Nanotechnology 2, (2003) 335.
¹² S. Choi, H. Yang, M. Chang, S. Baek, H. Hwang, S. Jeon, J. Kim, and C. Kim, Appl. Phys. Lett. 86, (2005) 251901.
¹³ P. Tognini, L. C. Andreani, M. Geddo, A. Stella, P. Cheyssac, R. Kofman, A. Migliori, Phys. Rev. B 53, (1996) 6992.
¹⁴ Q. Wan, C. L. Lin, W. L. Liu, and T. H. Wang, Appl. Phys. Lett. 82, (2003) 4708; Q. Wan, C. L. Lin, N. L. Zhang, W. L. Liu, G. Yang, T. H. Wang, Appl. Phys. Lett. 82, (2003) 3162.
¹⁵ D. I. Tetelbaum, A. N. Mikhaylov, O. N. Gorshkov, A. P. Kasatkin, A. I. Belov, D. M. Gaponova, and S. V. Morozov, Vacuum 78, (2005) 519.
¹⁶ I. Chamboleyron and A. R. Zanatta, J. Appl. Phys. 84 (1998) 1.

- ¹⁷ S. J. Wang, J. W. Chai, J. S. Pan, A. C. H. Huan, Appl. Phys. Lett. 89 (2006) 022105.
- ¹⁸ J. D. Eshelby, Proc. R. Soc. London A 241, (1957) 376.
- ¹⁹ S. Balasubramanian, G. Ceder, and K. D. Kolenbrander, J. Appl. Phys. 79, (1996) 4132.
- ²⁰ H.-Ch. Weissker, J. Furthmüller, and F. Bechstedt, Phys. Rev. B 65, (2002) 155328.
- ²¹ H.-Ch. Weissker, J. Furthmüller, and F. Bechstedt, Phys. Rev. B 67, (2003) 165322.
- ²² N. A. Efremov and S. I. Pokutnii, Soviet Phys. Solid St. 27, (1985) 27; *ibid.*, 32, (1990) 955.
- ²³ L. E. Brus, IEEE Trans. J. Quant. Electron. 22, (1986) 1909.
- ²⁴ M. V. Fischetti and J. M. Higman, *Monte Carlo Device Simulation: Full Band and Beyond*, edited by K. Hess Kluwer, Dordrecht, (1991).
- ²⁵ P. Hohenberg and W. Kohn, Phys. Rev. 136, (1964) B864.
- ²⁶ W. Kohn and L. J. Sham, Phys. Rev. 140, (1965) A1133.
- ²⁷ X. Gonze, J. M. Beuken, R. Caracas, F. Detraux, M. Fuchs, G. M. Rignanese, L. Sindic, M. Verstraete, G. Zerah, F. Jollet, M. Torrent, A. Roy, M. Mikami, P. Ghosez, J. Y. Raty, D. C. Allan, Comput. Mater. Sci. 25, (2002) 478.
- ²⁸ Y. P. Li and W. Y. Ching, Phys. Rev. B 31, (1985) 2172.
- ²⁹ Y. Xu and W. Y. Ching, Phys. Rev. B 44, (1991) 11048.
- ³⁰ Tetelbaum D I, Mikhaylov A N, Gorshkov O N, Kasatkin A P, Belov A I, Gaponova D M, and Morozov S V, Vacuum 78, (2005) 519; F. Liu, S. Garofalini, D. King-Smith, and D. Vanderbilt, Phys. Rev. B 49, (1994) 12528.
- ³¹ W Y Ching and Y N Xu, J. Am. Ceram. Soc., 77 (1994) 404.
- ³² Y. N. Xu and W. Y. Ching, Phys. Rev. B 51 (1995) 17379.
- ³³ S D Mo and W Y Ching, Phys. Rev. B, 57 (1998) 15219.
- ³⁴ T. Demuth, Y. Jeanvoine, J. Hafner, and J.G. Ángyán, J. Phys.: Condens. Matter 11, (1999) 3833.
- ³⁵ B. Holm, R. Ahuja, Y. Yourdshahyan, B. Johansson, and B. I. Lundqvist, Phys. Rev. B 59, (1999) 12777.
- ³⁶ D M Christie and J R Chelikowsky, Phys. Rev. B 62 (2000) 14703.
- ³⁷ J. C. Idrobo, H. Iddir, S. Ögüt, A. Ziegler, N. D. Browning, and R. O. Ritchie, Phys. Rev. B 72 (2005) 241301.
- ³⁸ S. Goedecker, M. Teter, and J. Huetter, Phys. Rev. B 54 (1996) 1703.
- ³⁹ J. P. Perdew and A. Zunger, Phys. Rev. B 23 (1981) 5048.
- ⁴⁰ D. M. Ceperley and B. J. Alder, Phys. Rev. Lett. 45 (1980) 566.
- ⁴¹ N. Troullier and J. L. Martins, Solid State Commun. 74, 613 (1990); Phys. Rev. B 43, 1993 (1991); Phys. Rev. B 43 (1991) 8861.
- ⁴² X. Gonze and C. Lee, Phys. Rev. B 55 (1997) 10355.
- ⁴³ R. W. G. Wyckoff, *Crystal Structure* (Interscience, New York, 1965).
- ⁴⁴ W. H. Baur and A. A. Khan, Acta Crystallogr. Sec. B-27 (1971) 2133.
- ⁴⁵ D. B. Balitskiĭ, O. Yu. Sil'vestrov, V. S. Balitskiĭ, Yu. V. Pisarevskii, D. Yu. Pushcharovskii, and E. Philippot, Crystallogr. Rep. 45 (2000) 145.
- ⁴⁶ A. A. Bolzan, B. Fong, J. B. Kennedy, and Ch. J. Howard, Acta. Crystallogr. Sect. B: Struct. Sci. B53 (1997) 373.
- ⁴⁷ H. Wang and G. Simmons, J. Geophys. Res. 78 (1973) 1262.
- ⁴⁸ L. Levien and C. T. Prewitt, Am. Mineral. 66 (1981) 324.
- ⁴⁹ R. T. Downs and D. C. Palmer, Am. Mineral. 79 (1994) 9.
- ⁵⁰ A. F. Wright and A. J. Leadbetter, Phil. Mag. 31 (1975) 1391.
- ⁵¹ M. Sugiyama, S. Endo, and K. Koto, Mineral. J. Japan 13 (1987) 455.
- ⁵² R. M. Van Ginhoven, H. Jónsson, and L. R. Corrales, Phys. Rev. B 71 (2005) 024208.
- ⁵³ J. Mckimin, P. Andreatch, and R. N. Thurston, J. Appl. Phys. 36 (1987) 1624.
- ⁵⁴ M. Grimsditch, A. Polian, V. Brazhkin, and D. Balitskiĭ, J. Appl. Phys. 83 (1998) 3018.
- ⁵⁵ D. J. Weidner, J. D. Bass, A. E. Ringwood, and W. Sinclair, Geophys. Res. Lett. 87 (1982) 4740.
- ⁵⁶ J. Watchman, Jr., E. E. Teft, D. G. Lam, Jr., and R. P. Stinchfield, J. Res. Natl. Bur. Stand. 64 (1960) 213.
- ⁵⁷ R. Vogelgesang, M. Grimsditch, and J. S. Wallace, Appl. Phys. Lett. 76 (2000) 982.
- ⁵⁸ J. A. Wendel and W. A. Goddard III, J. Chem. Phys. 97 (1992) 5048.
- ⁵⁹ *Theory of the Inhomogeneous Electron Gas*, edited by S. Lundqvist and N. H. March (Plenum, New York, 1983), and references therein.
- ⁶⁰ J. Sarnthein, A. Pasquarello, and R. Car, Phys. Rev. Lett. 74 (1995) 4682.
- ⁶¹ B K Ridley *Quantum Processes in Semiconductors* (Oxford University Press Oxford, 1999)
- ⁶² H. J. Monkhorst and J. D. Pack, Phys. Rev. B 13 (1976) 5188.
- ⁶³ L. E. Ramos, J. Furthmüller, and F. Bechstedt, Phys. Rev. B 69 (2004) 085102.
- ⁶⁴ W. L. Wyckoff, Am. J. Sci. 9 (1925) 448; 26 (2004) 33.
- ⁶⁵ W. L. Roberts *et al.*, *Encyclopedia of Minerals*, 2d ed. (New York, Van Nostrand Reinhold, 1990).
- ⁶⁶ R. H. French, J. Am. Ceram. Soc. 73 (1990) 447.
- ⁶⁷ Y. L. Page and P. Saxe, Phys. Rev. B 65 (2002) 104104.
- ⁶⁸ J. Weiss, Annu. Rev. Mater. Sci. 11 (1981) 381.
- ⁶⁹ J. Dong, O. F. Sankey, S. K. Deb, G. Wolf, and P. F. McMillan, Phys. Rev. B 61 (2000) 11979.